ISSN 0010-5082, Combustion, Explosion, and Shock Waves, 2018, Vol. 54, No. 6, pp. 737–746. © Pleiades Publishing, Ltd., 2018.
Original Russian Text © B.S. Jang, S.H. Lee, Y. Lee.

Blast Load Model Generating Multiple Impulse Curves for Different Scaled Distances

B. S. Jang[a], S. H. Lee[a], and Y. Lee[a]

UDC 523.593

Published in *Fizika Goreniya i Vzryva*, Vol. 54, No. 6, pp. 121–130, November–December, 2018.
Original article submitted July 31, 2017.

Abstract: This study proposes a blast load model that generates multiple impulse curves with appropriate shapes depending on the scaled distance and, thus, precisely calculates the blast load distribution over the structure surface. The suitability of the proposed model is examined by using the finite element simulation of a blast test with steel plates and comparing the predicted deflections with the measurements. The results reveal that the proposed model accurately calculates the blast load distribution over the structure surface. The predicted deflection profiles of the steel plates are closer to the measured deflection profiles when the proposed model is employed, as compared to the existing models, which produce only a single impulse curve.

Keywords: impulse curve, blast load, explosion, scaled distance, finite element simulation.

DOI: 10.1134/S001050821806014X

INTRODUCTION

When the incident pressure generated by the detonation of a high explosive (HE) hits the structure surface, it is reflected and reinforced, thus, producing reflected pressure. The reflected blast pressure becomes a blast load on the structure surface. In previous studies, the variation of the blast pressure at a point located at a certain distance in terms of time was referred to as the pressure–time history [1], pressure–time profile [2], and pressure history of a blast wave [3]. In this study, the term "pressure–time history" is adopted.

The time integration of the pressure–time history is the impulse at a point during a certain period of time. The impulse changes as the angle of incidence of the shock wave varies. The change in the impulse over the structure surface is known as the impulse curve, which is used to compute the blast load over the structure surface subjected to an explosion at a certain distance. Several research groups developed an algebraic formula of the impulse curve to compute the overall distribution of the blast load. Hereafter, the algebraic formula of the impulse curve is referred to as the blast load model for convenience.

Randers-Pehrson and Bannister [4] first introduced the blast load model and applied it to a 3D finite element (FE) code. Their model has a cosine function of the angle of incidence. Here, the angle of incidence is defined as the angle between the normal of the surface and the vector that points from the surface to the explosion source. Commercial FE codes, such as LS-Dyna [5], Abaqus [3], and Autodyn [6] adopted the blast load model proposed by Randers-Pehrson and Bannister (RPB model) [4]. The results of blast simulations using the RPB model were consistent with the experimental results for some cases [2, 7–10]. For some other cases, however, a noticeable difference was reported between the FE simulation and experimental results [11, 12].

Similarly, Dharmasena et al. [13] suggested a blast load model with a tangent function of the angle of incidence. They implemented their model in the Abaqus user subroutine to examine the dynamic response of square honeycomb core sandwich panels and solid plates manufactured from a super-austenite stainless steel al-

[a]Department of Mechanical Engineering, Chung-Ang University, Seoul, 156-756 Korea; ysl@cau.ac.kr.

loy, and compared the FE simulation results with the experimental observations. However, only the center deflection (but not the entire deflection profiles) of the test panels was compared with the experimental data. Consequently, the accuracy of the simulation could not be evaluated adequately.

The US protective construction manual TM 5-1300 [1] states that the shape of an impulse curve may change for different values of the scaled distance. However, the two models (RPB model [4] and Dharmasena model [13]) produce only a single impulse curve with a fixed shape regardless of the change in the scaled distance z, which is defined as the ratio of the standoff distance (r) to the cube root of the net explosive weight (w) ($z = r/w^{1/3}$ [m/kg$^{1/3}$]). Therefore, the blast load on the structure surface calculated by the two models might be significantly larger or smaller than the real blast load.

In this study, we propose a model that produces multiple impulse curves with appropriate shapes such that the distribution of the blast load over a structure surface can be calculated more accurately. The proposed model introduces a weighting function to the Dharmasena model [13]. The weighting function is expressed in an exponential form, which provides a continually decaying locus after reaching the maximum value. Thus, the weighting function regulates the shape of the impulse curve according to the scaled distance and multiple impulse curves are simultaneously generated.

In order to verify the usefulness of the proposed model, FE analyses were carried out using the Abaqus/Explicit code. The blast load distribution was computed by using a user subroutine VDLOAD wherein the proposed model and the polynomials proposed by Kingery and Bulmash [14] that calculate the pressure–time history were implemented. The FE simulation of quadrangular stiffened steel plates subjected to a blast was carried out, and the predicted deflection profiles of the plates were compared with the measured deflection profiles.

1. THEORETICAL BACKGROUND

1.1. Pressure–Time History and Reflected Impulse

The record of the blast pressure changes over time at the standoff point is called the pressure–time history (Fig. 1). Friedlander [15] suggested an idealized form of the pressure–time history and expressed it mathematically as

$$p(t) = p_{\text{atm}} + p_{\text{peak}}\left[1 - \frac{t}{t_d}\right]\exp\left(-\frac{bt}{t_d}\right), \qquad (1)$$

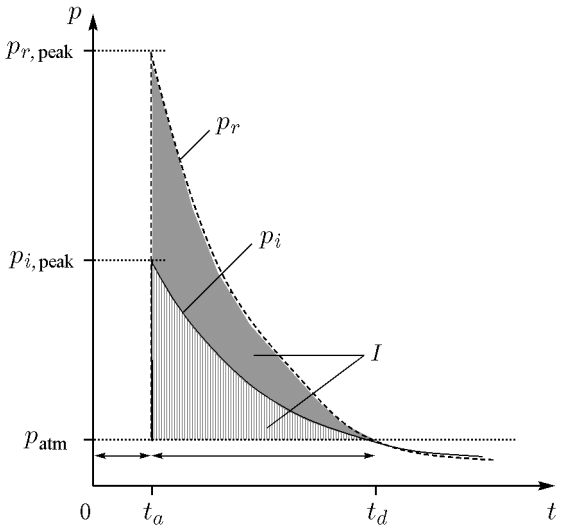

Fig. 1. Incident (p_i) and reflected (p_r) pressure–time history of an ideal blast wave; in domains indicated by I, the area is equal to the impulse.

where p_{atm} is the atmospheric pressure, p_{peak} is the peak (blast) pressure, t_d is the duration time of pressure, b is the pressure decay coefficient, and t is the time elapsed since the arrival of the blast wave. These blast parameters (p_{peak}, t_d, and b) corresponding to the scaled distance can be easily determined by using the Kingery–Bulmash polynomials [14]. After the pressure reaches the peak value, it decreases to the value of the atmospheric pressure at an exponential rate and further becomes smaller than the atmospheric pressure. The Kingery–Bulmash polynomials [14] were automated in a computer code called CONWEP, which is an algorithm that provides the blast parameters and calculates the pressure–time history with the input values of the explosive weight and standoff distance [16].

When the incident (blast) pressure hits a solid surface, it is reflected and reinforced, thus, producing the reflected pressure (see Fig. 1). The reflected pressure increases to a value 2–12 times greater than the incident pressure [1]. As the blast load is a dynamic load, the time must be considered when calculating the load. Thus, the blast load created on the structure surface owing to the reflected pressure is equal to the reflected impulse, which is calculated by the time integration of the reflected pressure–time history p_r:

$$I_r = \int_0^t p_r(t)dt, \qquad (2)$$

(I_r is the reflected impulse).

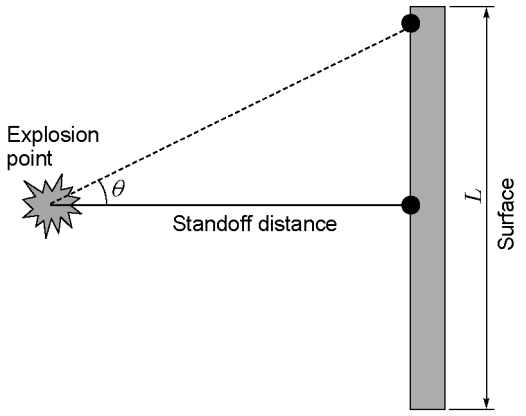

Fig. 2. Definition of the angle of incidence between the explosion point and the structure surface.

1.2. Existing Blast Load Models

The blast load, i.e., the reflected impulse over the structure surface, is not uniform owing to the characteristics of spherical propagation of the blast pressure. Randers-Pehrson and Bannister [4] described the distribution of the reflected impulse at arbitrary points of the structure surface subjected to an explosion by introducing a cosine function as

$$I_{\rm cr}(\theta) = I_r \cos^2\theta + I_i(1 + \cos^2\theta - 2\cos\theta), \qquad (3)$$

where I_r is the perpendicular ($\theta = 0$) reflected impulse, I_i is the perpendicular ($\theta = 0$) incident impulse, and θ is the angle of incidence. Figure 2 shows the definition of the angle of incidence between the normal of the structure surface and the vector that points from an arbitrary point on the surface of the structure to the explosion point. Hereafter, a blast load model is simply referred to as the model for the sake of convenience.

In the range of small scaled distances ($0.05 \leqslant z \leqslant 0.3$), the reflected pressure is 10 – 12 times greater than the incident pressure [1]. For this reason, Dharmasena et al. [13] ignored the perpendicular incident impulse and only considered the perpendicular reflected impulse to calculate $I_{\rm cr}(\theta)$:

$$I_{\rm cr}(\theta) = I_r \exp(-\tan^2\theta). \qquad (4)$$

Hereafter, the reflected impulse is simply referred to as the impulse for the sake of convenience.

In order to better understand the characteristics of the model, we utilized the ratio $I_{\rm cr}/I_r$. In this study, the graph of this ratio against the angle of incidence is referred to as a normalized impulse curve. Figure 3 shows the shapes of the normalized impulse curves generated from the two existing models (RPB model [4] and Dharmasena model [13]). A decrement of the normalized impulse with an increase in the angle of incidence indicates that the amount of the load at a remote

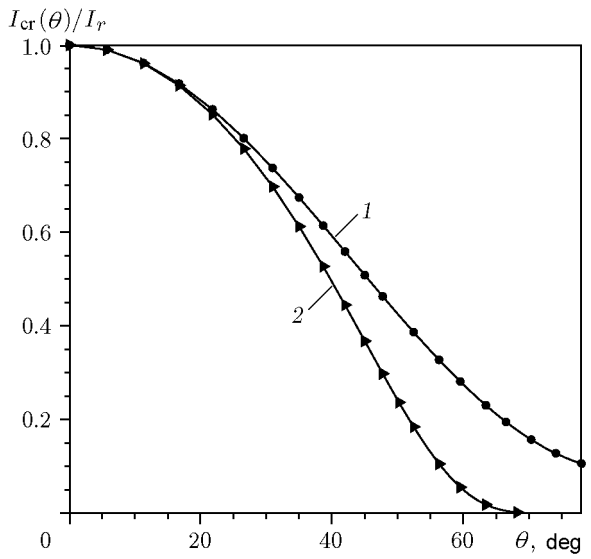

Fig. 3. Normalized impulse curves versus the angle of incidence: curve *1* shows the results predicted by the RPB model [4] for $I_{\rm cr}(\theta)/I_r = \cos^2\theta + (I_i/I_r)(1 + \cos^2\theta - 2\cos\theta)$ and $I_i = 0.1I_r$; curve *2* shows the results predicted by the Dharmasena model [13] for $I_{\rm cr}(\theta)/I_r = \exp(-\tan^2\theta)$.

point $\theta \neq 0$ from the middle point $\theta = 0$ is reduced as the angle of incidence increases. Hence, the normalized impulse curve can be understood as a distributed load acting on the structure surface.

The previous models (RPB model and Dharmasena model) produce single normalized impulse curves of fixed shapes regardless of the change in the scaled distance z as expressed in Eqs. (3) and (4), where z is absent. This indicates that the RPB and Dharmasena models may overestimate or underestimate the amount of the blast load on the structure surface if the scaled distance varies.

1.3. Proposed Blast Load Model

This study proposes a model that can produce multiple normalized impulse curves. Accordingly, a weighting function $\beta(z)$ is introduced to the Dharmasena model [13] such that the shapes of the normalized impulse curves vary if the scaled distance z changes. The proposed model is expressed as follows:

$$I_{\rm cr}(\theta, z) = I_r \exp(-\beta(z)\tan^2\theta). \qquad (5)$$

The weighting function is expressed in an exponential form, which provides a continually decaying locus after reaching the maximum value:

$$\beta = a[1 + b(z - c)]\exp(-b(z - c)) + d. \qquad (6)$$

The coefficients a, b, and c in Eq. (6) are determined by performing FE simulations of the stainless steel plate

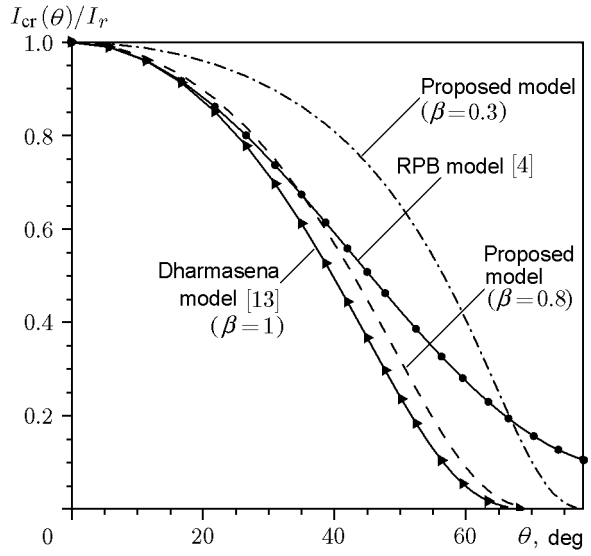

Fig. 4. Normalized impulse curves generated by the existing blast load models and by the proposed model.

blast test [13]. The value of d was chosen to be 20% of the limiting value of β.

Figure 4 shows two single normalized impulse curves generated by the existing blast load models [4, 13] and the multiple normalized impulse curves generated by the proposed model. As $\beta = 1$, as assumed in the existing models [4, 13], only a single normalized impulse curve is produced by each model. If β varies, the value of the exponent in Eq. (5) changes; subsequently, the shape of the normalized impulse curve is altered accordingly. Different values of β demonstrate that the net explosive weight changes for a fixed standoff distance and vice versa.

2. EXPERIMENT

In order to determine the coefficients of the weighting function in Eq. (6) and to validate the applicability of the proposed model, full-scale blast tests should be carried out. However, performing full-scale explosive tests is very expensive. Hence, the test results reported in previous studies [13, 17] were used instead.

2.1. Deformation of a Stainless Steel Plate Subjected to a Blast Load

Dharmasena et al. [13] carried out blast tests with square honeycomb core sandwich panels and solid test plates manufactured from high-ductility stainless steel [49Fe24Ni21Cr6Mo (wt.%)]. In this study, only the test results with solid test plates were used. Figure 5 shows

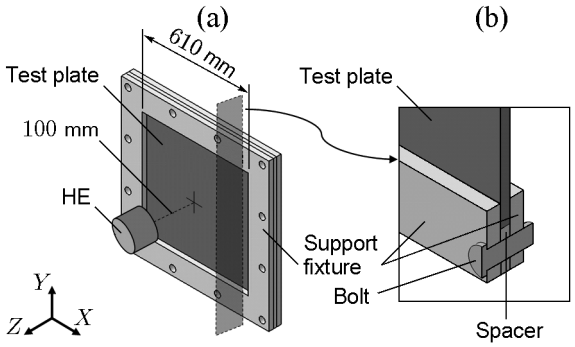

Fig. 5. Schematic of the blast tests [13] (the test plate thickness is 12.7 mm): (a) schematic; (b) cross-sectional view.

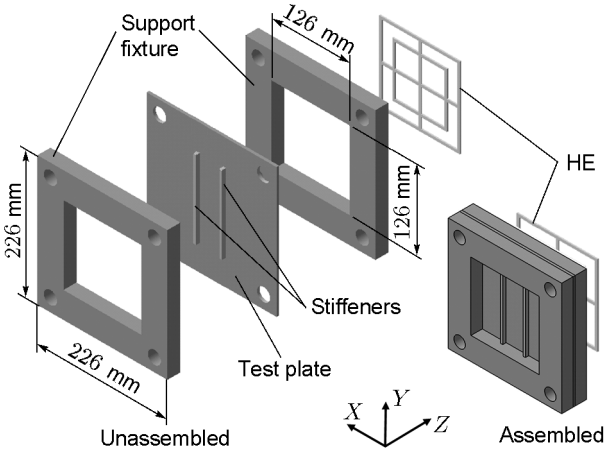

Fig. 6. Schematic of the blast tests [17] (the test plate thickness is 1.6 mm).

the schematic of the test. Explosives containing 1, 2, and 3 kg of TNT were placed at a distance of 100 mm from the plate center. The thickness of the solid test plates was 12.7 mm, and their length and width were 610 mm. The solid test plates were clamped between support fixtures, and spacers were placed between the solid test plate and the support fixtures.

2.2. Deformation of a Quadrangular Stiffened Plate Subjected to a Blast Load

Yuen and Nurick [17] performed blast experiments using square mild steel plates with quadrangular stiffeners attached (Fig. 6). The thickness of the test plates was 1.6 mm, and their length and width were 226 mm. The test plates were clamped between two support fixtures, and the area exposed to the blast was 126 × 126 mm. The PE4 plastic-bonded explosive (20.5 g) was shaped into a rectangular annulus (rectangular ring) and placed at a distance of 12 mm from the test plates. The stiffener configurations were flat (unstiffened), sin-

gle stiffener, double stiffener, cross-stiffener, and double cross-stiffener. The test results [17] were used to validate the applicability of the model proposed in this study. The unstiffened and double stiffened configurations were employed for the FE simulations.

3. TRANSIENT FINITE ELEMENT SIMULATION

Figure 7 shows the flow chart of the user subroutine VDLOAD used in this study to calculate the impulse values to be assigned to each node on the structure surface subjected to an explosion.

3.1. FE Simulation of the Dharmasena Test [13]

The blast source is kept at a standoff distance of 100 mm from the top surface of the plate (see Fig. 5). The explosive weight (1, 2, or 3 kg) given in the test setup was used as an input parameter. The corresponding scaled distances were found to be $z = 0.1$, 0.079, and 0.069 m/kg$^{1/3}$, respectively.

Only one-quarter of the plate was modeled with the center positioned at the origin of the X–Y plane, assuming the symmetry of the solution. All degrees of freedom (DOFs), including the rotational DOF, were fixed at the face boundaries $X = L_1$ and $Y = L_1$, where $L_1 =$ 305 mm. The X and Y symmetry boundary conditions were applied at the faces $X = 0$ and $Y = 0$, respectively (Fig. 5). The solid plate was discretized using C3D8R elements with five layers of elements across the plate. A total of 120 × 120 × 5 elements were used.

The Johnson–Cook model [18] was used to simulate the elastic-plastic behavior of the stainless steel plate with the following coefficients and constants: $A =$ 400 MPa, $B = 1500$ MPa, $C = 0.045$, $n = 0.4$, $m = 1.2$, and $\dot{\varepsilon}_0 = 0.001$ s^{-1}. The transition temperature was 293 K, and the melting temperature was 1800 K. The mechanical properties of the stainless steel plate were Young's modulus $E = 1.61 \cdot 10^5$ MPa, Poisson's ratio $\nu = 0.35$, and density $\rho = 7850$ kg/m^3 [19].

3.2. FE Simulation of the Yuen and Nurick Test [17]

In the Yuen and Nurick test setting [17], contrary to the Dharmasena test setting [13], 20.5 g of a plastic-bonded explosive (PE4), not TNT, was used. Furthermore, PE4 was shaped into two concentric rectangular annuli (see Fig. 6) and was positioned very close to the test plate (12 mm between the explosive and the test plate) so that a uniform blast load could be applied to the test plate. However, the blast load models [Eqs. (3)–(5)] assume that the blast load is produced by detonation of a point charge; hence, the equivalent standoff distance for the charge shaped as a rectangular annulus had to be calculated. The TNT equivalence of 20.5 g PE4 was determined first, based on the results of [20]; it turned out to be greater by a factor of 1.37.

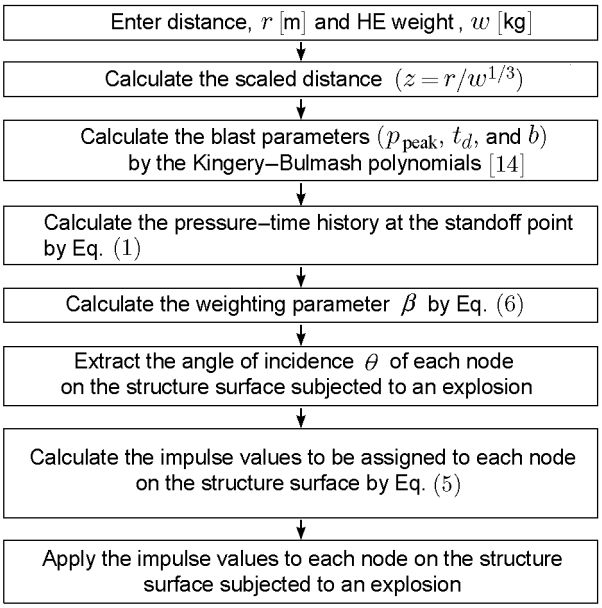

Fig. 7. Flow chart of the user subroutine VDLOAD used in this study.

In the Yuen and Nurick test [17], the measured impulse values were 31 and 37 N · s for the unstiffened plate and double stiffened plate, respectively. Substituting the measured impulse values and the calculated equivalent weight of TNT into the Kingery–Bulmash polynomials [14] yielded the scaled distances $z = 0.207$ and 0.187 m/kg$^{1/3}$. The equivalent standoff distances $r_e = 62.8$ and 56.8 mm were then calculated using the scaling law $z = r_e/w^{1/3}$.

Half of the square mild steel plate with quadrangular stiffeners attached was modeled with the plate center positioned at the origin of the X–Y plane. The plate with the quadrangular stiffeners was modeled by continuum C3D8R elements with five layers of elements across the plate. A total of 100 × 100 × 5 elements were used. All DOFs, including the rotational DOF, were fixed at the face boundary $X = L_2$, where $L_2 = 63$ mm. The Y-symmetry boundary conditions were applied at the $Y = 0$ face.

In the Yuen and Nurick test [17], the material deformation behavior was assumed to be rigid and viscoplastic. Hence, the Cowper–Symonds model [21] was used in this study to describe the deformation behavior of the mild steel plate at a given strain rate with

Mesh Convergence in the Dharmasena Test [13] and the Yuen and Nurick Test [17]

Number of elements	Maximum residual deflection, mm	CPU time, s
Dharmasena test [13]		
100 × 100 × 5	32.7	3892
120 × 120 × 5	33.5	5628
150 × 150 × 5	34.4	9971
200 × 200 × 5	34.2	23 386
Yuen and Nurick test [17]		
60 × 60 × 5	22.8	2481
80 × 80 × 5	23.4	4771
100 × 100 × 5	23.5	6451
150 × 100 × 5	23.7	18 146

the following coefficients and constants: $\sigma_y = 242$ MPa, $\dot{\varepsilon}_0 = 40$ s^{-1}, and $\eta = 5$. The mechanical properties of the mild steel plate were as follows: $E = 210$ GPa, $\nu = 0.33$, and $\rho = 7769$ kg/m^3.

For two FE simulations explained above, the mesh sensitivity was examined through a mesh convergence check. In order to find an adequate size of the mesh that yields an accurate result with acceptable computational cost, four different element sizes were compared for each FE model. The table shows the calculated maximum residual deflections of the test plate center and the CPU times required for different mesh configurations, respectively.

4. RESULTS AND DISCUSSION

4.1. Determination of the Coefficients in the Weighting Function

Figure 8 shows the computed and measured deflection profiles of the test plate in the Dharmasena test along a path from the center (point A) to the end (point B) of the test plate. The deflections at the point B predicted by FE simulation are perfectly zero. However, the measured deflections at the point B are not perfectly zero because the end of the test plate was clamped with bolts that are deformable during the test.

Figure 8a shows the measured and predicted deflection profiles for the HE weight of 1 kg ($z = 0.1$ m/kg$^{1/3}$). For $\beta = 0.9$, the predicted deflection profile is in close agreement with the experiments. The RPB model [4] greatly overestimates the deflection near the test plate

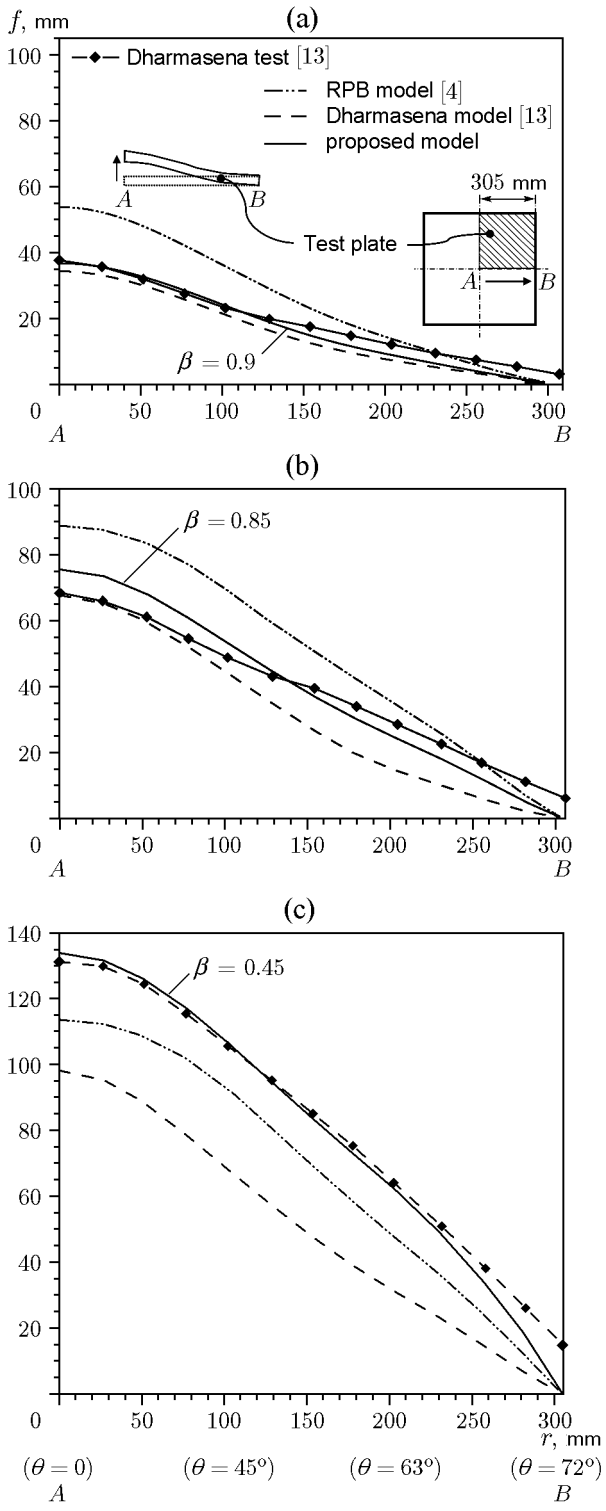

Fig. 8. Deflection (f) versus the distance (r) from the center to the end of the test plate subjected to an explosion of a TNT charge with a weight of 1 (a), 2 (b), and 3 kg (c).

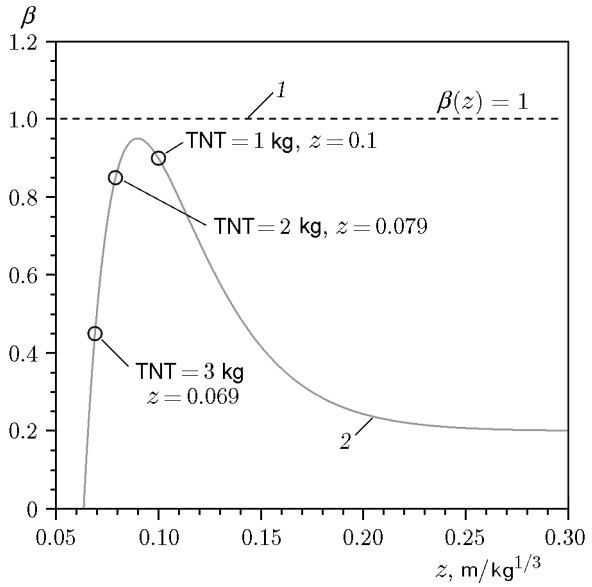

Fig. 9. Weighting function versus the scaled distance: curve *1* shows the results predicted by the Dharmasena model [13], $I_{\rm cr}(\theta) = I_r \exp(-1 \cdot \tan^2\theta)$; curve *2* shows the results predicted by the proposed model, $I_{\rm cr}(\theta, z) = I_r \exp(-\beta(z)\tan^2\theta)$ and $\beta = a[1 + b(z - c)]\exp(-b(z - c)) + d$.

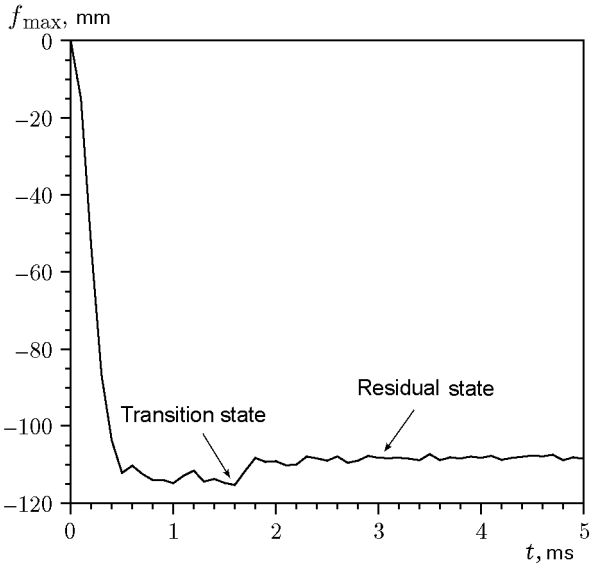

Fig. 10. FE analysis of the Dharmasena test [13]: maximum mid-point transient deflection as a function of time; the stainless steel plate thickness is 12.7 mm, the TNT charge weight is 3 kg, and the standoff distance is 100 mm.

center (point A), which indicates that the rate of the decrease of the normalized impulse curve generated by the RPB model is too slow as the angle of incidence θ increases (see Fig. 4). Meanwhile, the Dharmasena model [13] underestimates the deflection behavior because the normalized impulse curve generated by the Dharmasena model decreases rapidly beginning from $\theta \approx 40^\circ$ as shown in Fig. 4.

In Fig. 8b, the measured and predicted deflection profiles are presented for the HE weight of 2 kg ($z = 0.079$ m/kg$^{1/3}$). In this case, the Dharmasena model [13] considerably underestimates the deflection, whereas the RPB model [4] appreciably overestimates both the experimental deflection profile and that in Fig. 8a. A possible reason is the behavior of the normalized impulse curves generated by these model, as was noted above (see Fig. 4). The deflection profile computed by the proposed model ($\beta = 0.85$) is in good agreement with the measured deflection. With the proposed model, the underestimation and overestimation of the deflection are less pronounced than those ensured by the Dharmasena and RPB models. This is because the normalized impulse curve, i.e., the blast load, was computed appropriately by the proposed model.

Figure 8c shows the measured and predicted deflection profiles for the HE weight of 3 kg ($z = 0.069$ m/kg$^{1/3}$). While the RPB model [4] underestimates the deflection, the Dharmasena model underestimates the deflection behavior even more seriously. The proposed model ($\beta = 0.45$) is in close agreement with the experimental result. This is because the normalized impulse curves generated by the Dharmasena model [13] model and RPB model [4] drop considerably more rapidly than that generated by the model proposed in the present study. This means that the existing models are not able to capture the change in the impulse curve due to the variation of the scaled distance.

Thus, $\beta = 0.9$, 0.85, and 0.45 corresponding to the scaled distances $z = 0.1$, 0.079, and 0.069 m/kg$^{1/3}$ were determined. Figure 9 shows the weighting function in terms of the scaled distance $\beta(z)$ based on these results; β was assumed to decrease exponentially after reaching the maximum value.

The weighting function [Eq. (6)] was determined as

$$\beta = 0.75[1 + 41.3(z - 0.090)] \times \exp[-41.3(z - 0.090)] + 0.20. \quad (7)$$

The value of 0.20 is 20% of the limiting value of β.

4.2. Dynamic Response of the Stainless Steel Plate

Figure 10 shows the unsteady process in which a 12.7-mm thick stainless steel plate is deformed. Variations of the maximum mid-point deflection of the plates as a function of time are illustrated.

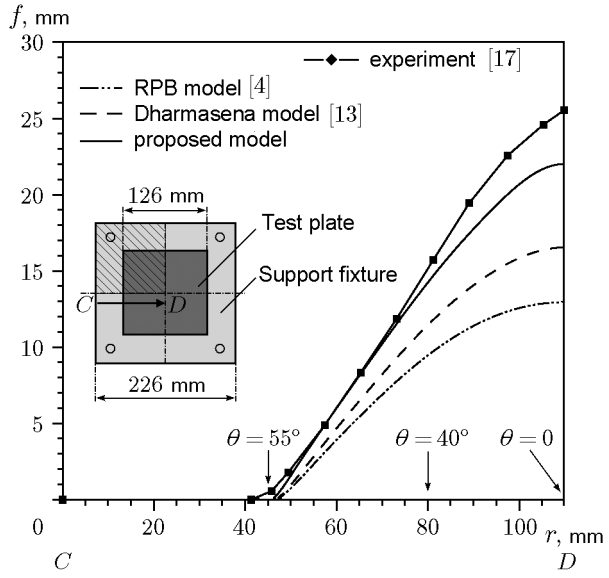

Fig. 11. Comparison of the simulated and experimental results for the deflection of the unstiffened test plate subjected to an explosion of a PE4 charge (20.5 g).

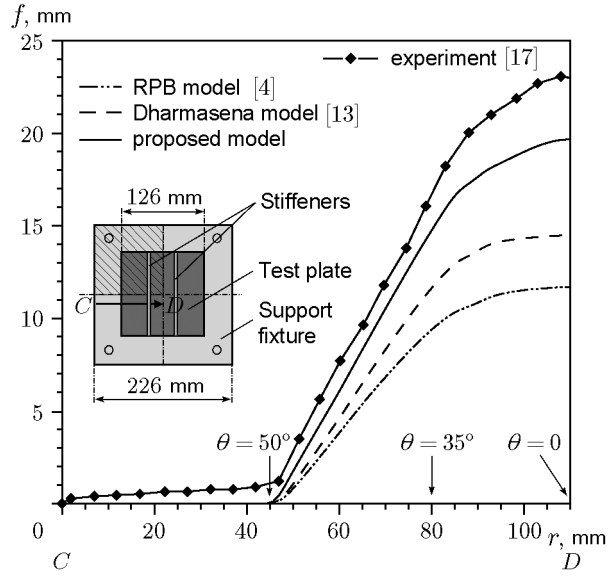

Fig. 12. Comparison of the simulated and experimental results for the deflection of the double stiffened test plate subjected to an explosion of a PE4 charge (20.5 g).

The plastic deflection response is dominant because the steel plate is subjected to an explosion of a 3-kg TNT charge from a standoff distance of 100 mm. Hence, the difference between the maximum mid-point deflection and the residual mid-point deflection, i.e., springback, is approximately 10 mm. The deflection reaches its maximum transient magnitude at 1.6 ms, and then transient defection is stabilized to the residual magnitude at about 3 ms. Oscillations at the early stage are not large. This is because the plate is deformed by a relatively large explosive power from a relatively short standoff distance.

4.3. Verification of the Proposed Model

We performed FE simulations of the Yuen and Nurick blast test [17] to verify the model proposed in this study. The test conditions of the Yuen and Nurick test were exactly reflected in the FE simulations. The blast load was generated by the user subroutine VDLOAD, in which the proposed model was implemented.

Figure 11 shows the measured and predicted deflection profiles along a path from the boundary (point C) to the center (point D) of the unstiffened plate, i.e., with no stiffener attached to the test plate. The scaled distance is $z = 0.207$ m/kg$^{1/3}$. Compared to the deflection profiles produced by the other models, the deflection obtained by the proposed model is in very good agreement with the measurements from about 45 mm (corresponding to $\theta = 55°$) to ≈80 mm ($\theta = 40°$). Regarding the maximum differences, the Dharmasena model [13] underestimates the deflection by 37%, and the deflection value predicted by the RPB model [4] is even smaller. The maximum difference is −49.1 %. However, the maximum difference diminishes to −14.4% when the proposed model is implemented. Even though the double stiffened test plate has a slightly different test plate configuration compared to the unstiffened plate, the proposed model still yields reasonable results. Therefore, it is deduced that the proposed model can be applied to the blast FE analyses of a plate reinforced with stiffeners that have different cross sections and different arrangements. However, there is an application limit because the proposed model cannot be applied if the plate has a curved surface. The proposed model can be applied only if the plate surface is flat. Nevertheless, the stiffeners can be attached behind the flat surface over which the blast load is applied.

Figure 12 shows the measured and predicted deflection profiles of a double stiffened test plate in which two stiffeners are attached. The scaled distance is 0.187 m/kg$^{1/3}$. Compared to the deflection profiles produced by the other models, the deflection profile predicted by the proposed model shows a fairly close accordance with the measurements from about 45 mm ($\theta = 50°$) to ≈80 mm ($\theta = 35°$). In order to quantify the usefulness of the proposed model, the maximum differences between the measurements and predictions are evaluated at the plate center (point D). The Dhar-

masena model [13] significantly underestimates the deflection by 35.6%. The underestimation of the deflection by the RPB model [4] is even more serious (49.6%). However, the maximum difference is reduced to 14.3% when the proposed model is implemented. Therefore, the proposed model seems to produce relatively accurate results because the suitable normalized impulse curve is obtained according to the scaled distance z, and the amount of the blast load is thus calculated correctly. This result shows that the proposed model can be used within a scaled distance range from 0.069 to 0.207 m/kg$^{1/3}$.

CONCLUSIONS

In this study, we proposed a model that produces multiple normalized impulse curves of appropriate shapes by introducing a weighting function to the Dharmasena model [13]. The applicability of the proposed model was validated by performing FE simulations of the dynamic response (deflection) of quadrangular stiffened steel plates subjected to a blast load and by comparing the predicted deflection behavior with the experimental results. The conclusions can be formulated as follows.

1. The proposed model can precisely compute the blast load distribution over the surface of a structure even when the scaled distance changes. The predictive ability of the dynamic response of quadrangular stiffened steel plates increased approximately by 35% when the proposed model was used.

2. Therefore, the proposed model can be useful for blast FE simulations with any type of the steel plate configuration if the scaled distance is within the range of 0.069–0.207 m/kg$^{1/3}$ and the surface of the steel plate is flat.

3) The applicability of the proposed model can be extended if more explosion test data are acquired in the future studies.

This research was supported by the Chung-Ang University Graduate Research Scholarship in 2015 and by the National Research Foundation of Korea grant funded by the Korea government (Ministry of Science, Information and Communication Technology) (Grant No. NRF-2016R1D1A1B03935327).

REFERENCES

1. "Structures to Resist the Effects of Accidental Explosions," Technical Manual 5-1300 (U. S. Department of the Army, 1990).
2. T. Børvik, A. G. Hanssen, M. Langseth, and L. Olovsson, "Response of Structures to Planar Blast Loads—A Finite Element Engineering Approach," Comput. Struct. **87**, 507–520 (2009).
3. *SIMULIA. Abaqus Analysis User's Manual*, Vol. 1 (2012).
4. G. Randers-Pehrson and K. A. Bannister, *Airblast Loading Model for DYNA2d and DYNA3d* (Army Research Laboratory, 1997).
5. *LS-DYNA Keyword User's Manual*, Version 971 (Livermore Software Technol. Corp., 2007).
6. *Autodyn User's Manual* (ANSYS Inc.,2013).
7. V. H. Balden and G. N. Nurick, "Numerical Simulation of the Post-Failure Motion of Steel Plates Subjected to Blast Loading," Int. J. Impact Eng. **32** (1), 14–34 (2005).
8. G. S. Langdon and G. K. Schleyer, "Deformation and Failure of Profiled Stainless Steel Blast Wall Panels. Pt. III: Finite Element Simulations and Overall Summary," Int. J. Impact Eng. **32** (6), 988–1012 (2006).
9. L. Mazurkiewicz, J. Malachowski, P. Baranowski, and K. Damaziak, "Comparison of Numerical Testing Methods in Terms of Impulse Loading Applied to Structural Elements," Theor. Appl. Mech. **51** (3), 615–625 (2013).
10. K. Sprangher, I. Vasilakos, D. Lecompte, H. Sol, and J. Vantomme, "Numerical Simulation and Experimental Validation of the Dynamic Response of Aluminum Plates under Free Air Explosions," Int. J. Impact Eng. **54** (1), 83–95 (2003).
11. B. Zakrisson, B. Wikman, and H. Häggblad, "Numerical Simulations of Blast Loads and Structural Deformation from Near-Field Explosions in Air," Int. J. Impact Eng. **38** (7), 597–612 (2011).
12. T. A. Hustad and A. L. Lindland, *Aluminum Structures Exposed to Blast Loading* (Norwegian Univ. Sci. Tech., 2014).
13. K. P. Dharmasena, H. N. G. Wadley, Z. Xue, and J. W. Hutchinson, "Mechanical Response of Metallic Honeycomb Sandwich Panel Structures to High Intensity Dynamic Loading," Int. J. Impact Eng. **35**, 1063–1074 (2008).
14. C. N. Kingery and G. Bulmash, *Airblast Parameters from TNT Spherical air Burst and Hemispherical Surface Burst* (U. S. Army Ballistic Research Laboratory, Aberdeen Proving Ground, 1984).
15. F. G. Friedlander, "The Diffraction of Sound Pulses. I. Diffraction by a Semi-Infinite Plane," Proc. Roy. Soc. London, A **186**, 322–344 (1946).
16. *Fundamentals of Protective Design for Conventional Eeapons, Technical Manual* (U. S. Department of the Army, 1986).

17. S. C. Yuen and G. N. Nurick, "Experimental and Numerical Studies on the Response of Quadrangular Stiffened Plates. Pt I: Subjected to Uniform Blast Load," Int. J. Impact Eng. **31** (1), 55–83 (2005).
18. G. R. Johnson and W. H. Cook, "A Constitutive Model and Data for Metals Subjected to Large Strain, High Strain Rates and High Temperatures," in *Proc. 7th Int. Symp. on Ballistics*, (1983), Vol. 54, pp. 541–547.
19. K. Nahshon et al., "Dynamic Shear Rupture of Steel Plates," J. Mech. Mat. Struct. **2** (10), 2049–2066 (2007).
20. S. E. Rigby and P. W. Sielicki, "An Investigation of TNT Equivalence of Hemispherical PE4 Charges," Eng. Trans. **62**, 423-35 (2014).
21. G. Cowper and P. S Symonds, *Strain-Hardening and Strain-Rate Effects in the Impact Loading of Cantilever Beams* (Brown Univ., U.S.A., 1957).